Comparison of Modeled to Observed Global Irradiance*

RICHARD F. DAVIS†

NOAA/Alaska Fisheries Science Center, Seattle, Washington

(Manuscript received 7 March 1995, in final form 2 August 1995)

ABSTRACT

The accuracy of a spectral, clear-sky model to predict hourly global irradiance was investigated using radiation and meteorological observations collected at the Seattle–Tacoma airport between 1 January 1988 and 31 October 1991. The model was first run using the 1976 U.S. standard atmosphere values as inputs, then using the local atmospheric conditions. Clear-sky irradiance values generated by both atmospheres, standard and local, were attenuated using local cloud cover observations for comparison with measured irradiance. Values and trends of the statistical descriptors for the two atmospheres were almost identical. Overall, the model overestimated observed irradiance by less than 6%. Cloud cover was the major source of deviation between the modeled and observed values. The close correspondence between the two model runs suggests that the U.S. standard atmosphere, in conjunction with global cloud datasets, can be used in spectral models to generate irradiance at remote locations.

1. Introduction

Oceanographic models for estimating rates of primary production and for the spaceborne remote sensing of ocean color require solar energy as one input (e.g., Platt and Sathyendranath 1988). It is, however, impractical to continuously measure radiation over the vast majority of the ocean. Over the years several broadband models of irradiance have been developed that possess varying degrees of accuracy (Davies and McKay 1982; Iqbal 1983; Davies and McKay 1989; Gueymard 1993). The alternative, spectral models, are more mechanistic than broadband models because they utilize the known extraterrestrial spectral distribution of solar energy and the inherent optical properties of atmospheric constituents. Oceanographic primary production models utilizing spectral absorption characteristics of phytoplankton would be enhanced by the use of accurate spectral irradiance models (Morel 1991; Berthon and Morel 1992). When testing the ability of these spectral models to predict irradiance, researchers typically measure the meteorological input variables at the same time that they measure irradiance (Bird 1984; Justus and Paris 1985; Bird and Riordan 1986, hereafter referred to as BR; Louche et al. 1988; Gregg and Carder 1990; Nann and Riordan 1991). For routine use of a model at a remote location this practice of measuring all inputs in real time is neither feasible nor desirable. One solution is to use the U.S. standard atmosphere (NOAA 1976, hereafter referred to as USSA) as the model inputs. Another would be to use the local atmospheric (LA) conditions as indicated by meteorological data routinely collected at National Weather Service (NWS) observatories if one is sufficiently close to the site of interest. In this study, the BR spectral, clear-sky model was modified to take into account cloud cover and then compared its output to observed global irradiance measured at the Seattle–Tacoma (Sea–Tac) airport. The model was run twice, each with a different atmosphere, the inputs being first the USSA and then the observed meteorological variables for Sea–Tac archived with the National Climatic Data Center (NCDC), Asheville, North Carolina. (A list of symbols and abbreviations is provided in Table 1.)

2. Data sources and processing

Observed hourly global irradiance values (E) and corresponding meteorological observations from 1 January 1988 to 31 October 1991 were obtained from the NCDC. Observed irradiance values are the hourly means for the preceding hour and are obtained by summing 1-min samples over the observation hour and dividing by 60. All other meteorological variables are instantaneous observations taken within 10 min of the recorded hour. Predicted irradiance estimates ($\hat{E}_S$ for

* NOAA Fisheries–Oceanography Coordinated Investigations Contribution Number FOCI-0252.

† Current affiliation: Oregon State University, College of Oceanic and Atmospheric Sciences, Corvallis, Oregon.

Corresponding author address: Richard F. Davis, Alaska Fisheries Science Center, NOAA/NMFS, BIN C 15700, Bldg. #4, 7600 Sand Point Way NE, Seattle, WA 98115-0070.

TABLE 1. Symbols and abbreviations.

Symbol	Description
α	Ångström wavelength exponent
β	Ångström turbidity coefficient
A	cloud factor exponent
B	cloud factor coefficient
BR	Bird and Riordan (1986)
COADS	Comprehensive Ocean–Atmosphere Data Set
E (kJ m^{-2} h^{-1})	observed irradiance
$\hat{E}_S$ (kJ m^{-2} h^{-1})	modeled irradiance using standard atmosphere
$\hat{E}_L$ (kJ m^{-2} h^{-1})	modeled irradiance using local atmosphere
$\bar{E}$ (0) (kJ m^{-2} h^{-1})	Mean observed clear-sky irradiance
LA	local atmosphere from meteorological observations
MBE (kJ m^{-2} h^{-1})	mean bias error
NCDC	National Climatic Data Center
NOAA	National Oceanic and Atmospheric Administration
NWS	National Weather Service
r^2	squared correlation coefficient
rmse (kJ m^{-2} h^{-1})	root-mean-square error
t_d (°C)	dewpoint temperature
TOSC (tenths)	total opaque sky cover
USSA	1976 U.S. standard atmosphere
V (km)	horizontal visibility
w' (cm)	precipitable water

USSA and $\hat{E}_L$ for local meteorological observations) are instantaneous values centered on the half-hour of the recorded hour.

The data have been quality controlled by the NCDC and checked for internal consistency, for serial consistency, and against defined limits for various meteorological variables (NCDC 1991). Values failing the control tests were flagged by the NCDC. In this study a data record was removed from consideration for any of the following reasons: if it had been flagged by the NCDC; observed global irradiance was 0 kJ m^{-2} h^{-1}; measured direct normal irradiance was greater than measured global irradiance; any meteorological or irradiance observation was missing; horizontal visibility was less than 5 km; or solar zenith angle was greater than 80°. After reduction there were 11 371 hourly observations remaining from the original 33 600.

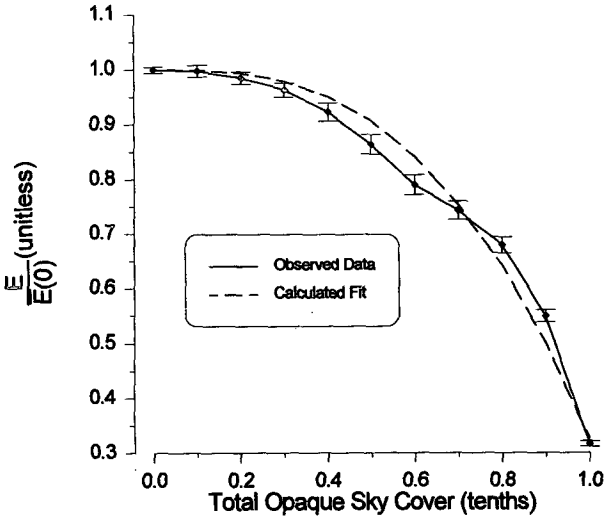

FIG. 1. Mean ratios of observed global irradiance E to the corresponding mean clear-sky $\bar{E}$ (0) as function of total opaque sky cover (TOSC). Error bars are the 95% confidence limits. The dashed line is the best-fit curve from Eq. (4).

The pyranometer used at the Seattle–Tacoma airport was an Eppley[1] PSP until 29 September 1989 and a SpectroSun SR-75 for the remainder of the study period. Each instrument was calibrated every 6 months and has an expected measurement uncertainty of 3% (D. Nelson 1992, personal communication).

3. Model

The spectral irradiance model used in this study was the version described by BR, which calculates global irradiance by summing two estimated components: direct and diffuse irradiance. Clear-sky global irradiance values produced by the model were then modified to take into account local cloud cover. To match the spectral response of the pyranometers used to collect data at the Seattle–Tacoma airport, the output of the model

[1] Reference to trade names does not imply endorsement by the National Marine Fisheries Service, NOAA.

TABLE 2. Model inputs.

Variable	Local source	USSA value
Air temperature (°C)	NCDC	15.0
Ångström turbidity coefficient	Shettle and Fenn (1975)	0.1296
Ångström wavelength exponent	Shettle and Fenn (1975)	1.038
Atmospheric pressure (kPa)	NCDC	1013.25
Ground albedo	SOLMET V2	0.165
Ozone (atm cm)	Van Heukolon (1979)	0.34
Precipitable water (cm)	Atwater and Ball (1976)	1.74
Total opaque sky cover (tenths)	NCDC	NCDC

TABLE 3. Statistical descriptors for USSA. Units for mean irradiance values, mean bias error (MBE), and root-mean-square error (rmse) are kilojoules per square meter per hour; all other entries are unitless.

		Mean ± standard error						
	N	Observed	Modeled	MBE	MBE (%)	rmse	rmse (%)	r^2
All	11 371	1168 ± 8	1224 ± 8	56	4.8	286	24.5	0.899
TOSC	N	Observed	Modeled	MBE	MBE (%)	rmse	rmse (%)	r^2
0.0	1731	1843 ± 20	1926 ± 21	83	4.5	177	9.6	0.968
0.1	651	1745 ± 34	1829 ± 34	83	4.8	193	11.1	0.960
0.2	671	1691 ± 32	1789 ± 33	98	5.8	227	13.4	0.943
0.3	635	1666 ± 34	1763 ± 34	97	5.8	254	15.3	0.925
0.4	509	1638 ± 37	1764 ± 37	126	7.7	318	19.4	0.881
0.5	452	1565 ± 39	1705 ± 37	140	8.9	358	22.9	0.843
0.6	497	1409 ± 36	1543 ± 34	134	9.5	375	26.6	0.814
0.7	608	1319 ± 31	1392 ± 28	74	5.6	373	28.3	0.771
0.8	741	1174 ± 27	1157 ± 22	−17	−1.5	379	32.3	0.733
0.9	1012	926 ± 19	881 ± 14	−45	−4.9	329	35.6	0.714
1.0	3864	496 ± 7	529 ± 5	33	6.7	278	56.0	0.536
Zenith angle	N	Observed	Modeled	MBE	MBE (%)	rmse	rmse (%)	r^2
25°–30°	762	2339 ± 32	2359 ± 31	20	0.9	447	19.1	0.754
31°–35°	670	2201 ± 32	2272 ± 32	71	3.2	416	18.9	0.768
36°–40°	838	1968 ± 27	2022 ± 27	54	2.7	383	19.5	0.778
41°–45°	712	1845 ± 29	1947 ± 27	102	5.6	369	20.0	0.788
46°–50°	1064	1520 ± 22	1601 ± 20	81	5.3	342	22.5	0.782
51°–55°	841	1385 ± 22	1469 ± 21	84	6.1	292	21.1	0.803
56°–60°	1163	1113 ± 16	1184 ± 15	71	6.3	278	25.0	0.759
61°–65°	1046	873 ± 15	944 ± 14	71	8.1	228	26.1	0.788
66°–70°	1565	644 ± 9	692 ± 8	47	7.3	190	29.5	0.740
71°–75°	1407	468 ± 8	506 ± 7	38	8.2	151	32.3	0.731
76°–80°	1303	313 ± 5	322 ± 4	8	2.7	107	34.2	0.664
Month	N	Observed	Modeled	MBE	MBE (%)	rmse	rmse (%)	r^2
Jan	636	438 ± 12	469 ± 12	31	7.2	144	32.9	0.795
Feb	676	713 ± 20	749 ± 19	36	5.1	208	29.1	0.847
Mar	917	1009 ± 22	1073 ± 22	64	6.3	284	28.2	0.836
Apr	1209	1220 ± 24	1288 ± 24	67	5.5	305	25.0	0.879
May	1375	1341 ± 25	1386 ± 24	46	3.4	334	24.9	0.869
Jun	1425	1419 ± 26	1456 ± 24	38	2.6	379	26.7	0.852
Jul	1368	1628 ± 27	1699 ± 27	72	4.4	308	18.9	0.911
Aug	1136	1473 ± 26	1551 ± 26	78	5.3	308	20.9	0.890
Sep	1016	1357 ± 23	1432 ± 24	76	5.6	220	16.2	0.926
Oct	692	840 ± 21	904 ± 21	64	7.6	239	28.5	0.833
Nov	521	472 ± 14	507 ± 14	36	7.6	157	33.2	0.787
Dec	400	382 ± 13	398 ± 11	16	4.1	130	33.9	0.759

was integrated from 0.3 to 2.8 μm. While complete details can be found in BR, a brief description of the model is given below.

Direct irradiance was estimated by attenuating the extraterrestrial spectral irradiance by molecular (Rayleigh) scattering, aerosol scattering, and absorption, water vapor absorption, ozone absorption, and uniformly mixed gas absorption. Table 2 lists the sources of values in the two model runs, including the USSA values. Rayleigh scattering was a function of the optical pathlength, determined by the station atmospheric pressure and solar zenith angle (Kneizys et al. 1980). Spectral aerosol transmittance $\tau_{a\lambda}$ was estimated as described by the Ångström turbidity formula (see Ångström 1961 for review):

$$\tau_{a\lambda} = \exp(-\beta\lambda^{-\alpha}M), \quad (1)$$

where β is the aerosol turbidity coefficient, λ (μm) is wavelength, α is the Ångström exponent, and M is the relative optical air mass as given by Kasten (1966). For LA the rural aerosol model (Shettle and Fenn 1975) was used, where α is equal to 1.0274 for wavelengths $\lambda < 0.5$ μm and 1.2060 for $\lambda \geq 0.5$ μm. Here β was determined using the formula of Selby and McClatchey (1975):

TABLE 4. Statistical descriptors for LA. Units for mean irradiance values, mean bias error (MBE), and root-mean-square error (rmse) are kilojoules per square meter per hour; all other entries are unitless.

		Mean ± standard error						
	N	Observed	Modeled	MBE	MBE (%)	rmse	rmse (%)	r^2
All	11 371	1168 ± 8	1233 ± 8	65	5.5	287	24.6	0.901
TOSC	N	Observed	Modeled	MBE	MBE (%)	rmse	rmse (%)	r^2
0.0	1731	1843 ± 20	1956 ± 21	114	6.2	186	10.1	0.971
0.1	651	1745 ± 34	1858 ± 34	112	6.4	199	11.4	0.964
0.2	671	1691 ± 32	1818 ± 33	126	7.5	238	14.1	0.943
0.3	635	1666 ± 34	1787 ± 34	122	7.3	269	16.2	0.922
0.4	509	1638 ± 37	1784 ± 37	146	8.9	327	19.9	0.881
0.5	452	1565 ± 39	1716 ± 37	151	9.7	363	23.2	0.843
0.6	497	1409 ± 36	1561 ± 34	152	10.8	382	27.1	0.814
0.7	608	1319 ± 31	1408 ± 28	89	6.8	376	28.5	0.771
0.8	741	1174 ± 27	1167 ± 22	−8	−0.7	378	32.2	0.733
0.9	1012	926 ± 19	880 ± 14	−46	−5.0	329	35.5	0.716
1.0	3864	496 ± 7	517 ± 5	22	4.3	270	54.4	0.559
Zenith angle	N	Observed	Modeled	MBE	MBE (%)	rmse	rmse (%)	r^2
25°–30°	762	2339 ± 32	2363 ± 31	24	1.0	443	18.9	0.760
31°–35°	670	2201 ± 32	2276 ± 32	76	3.4	415	18.9	0.773
36°–40°	838	1968 ± 27	2025 ± 27	57	2.9	380	19.3	0.786
41°–45°	712	1845 ± 29	1952 ± 28	107	5.8	370	20.1	0.791
46°–50°	1064	1520 ± 22	1607 ± 21	87	5.7	343	22.5	0.787
51°–55°	841	1385 ± 22	1476 ± 21	91	6.6	294	21.2	0.807
56°–60°	1163	1113 ± 16	1193 ± 15	80	7.2	278	25.0	0.769
61°–65°	1046	873 ± 15	957 ± 14	84	9.6	233	26.6	0.794
66°–70°	1565	644 ± 9	704 ± 9	59	9.2	196	30.3	0.744
71°–75°	1407	468 ± 8	520 ± 8	52	11.2	157	33.5	0.741
76°–80°	1303	313 ± 5	333 ± 5	20	6.3	111	35.4	0.661
Month	N	Observed	Modeled	MBE	MBE (%)	rmse	rmse (%)	r^2
Jan	636	438 ± 12	486 ± 13	48	11.0	154	35.1	0.795
Feb	676	713 ± 20	770 ± 20	57	8.0	211	29.6	0.855
Mar	917	1009 ± 22	1104 ± 23	95	9.4	294	29.1	0.842
Apr	1209	1220 ± 24	1303 ± 25	83	6.8	311	25.5	0.881
May	1375	1341 ± 25	1398 ± 24	58	4.3	336	25.1	0.870
Jun	1425	1419 ± 26	1464 ± 24	45	3.1	375	26.4	0.856
Jul	1368	1628 ± 27	1707 ± 27	79	4.9	307	18.9	0.912
Aug	1136	1473 ± 26	1541 ± 26	68	4.6	300	20.4	0.893
Sep	1016	1357 ± 23	1426 ± 24	69	5.1	221	16.3	0.925
Oct	692	840 ± 21	900 ± 21	60	7.2	236	28.1	0.837
Nov	521	472 ± 14	519 ± 15	47	10.0	163	34.5	0.794
Dec	400	382 ± 13	415 ± 13	33	8.6	134	35.2	0.773

$$\beta = (0.55)^{\alpha}\left(\frac{3.912}{V} - 0.01162\right) \times [0.02472(V - 5) + 1.132], \quad (2)$$

where V (km) is horizontal visibility.

For water vapor, ozone, and uniformly mixed gas transmittance, Leckner's (1978) equations and absorption coefficients as reported and modified by BR were used. Concentrations of the constituents were determined from various sources. Water vapor for the USSA run was set to the mean value for the United States of 1.74 (Reitan 1960). The LA water vapor was determined from Atwater and Ball's (1976) simplified equations of Smith (1966):

$$w' = \exp(0.07074t_d + y), \quad (3)$$

where w' (cm) is the uncorrected precipitable water, t_d (°C) is dewpoint temperature, and y is equal to −0.02290 from April to June and 0.02023 for all other months. Ozone concentration was modeled according to Van Heuklon (1979) and used in the ozone mass expression of Robinson (1966) as given by Iqbal (1983). Uniformly mixed gas transmittance was formulated as a function of pressure-corrected air mass.

Diffuse irradiance was calculated according to BR. Ground albedo for the USSA run was set at 0.165, an average value for pavement (Iqbal 1983). For the LA run, ground albedo was not treated as a constant but was allowed to vary monthly according to the values

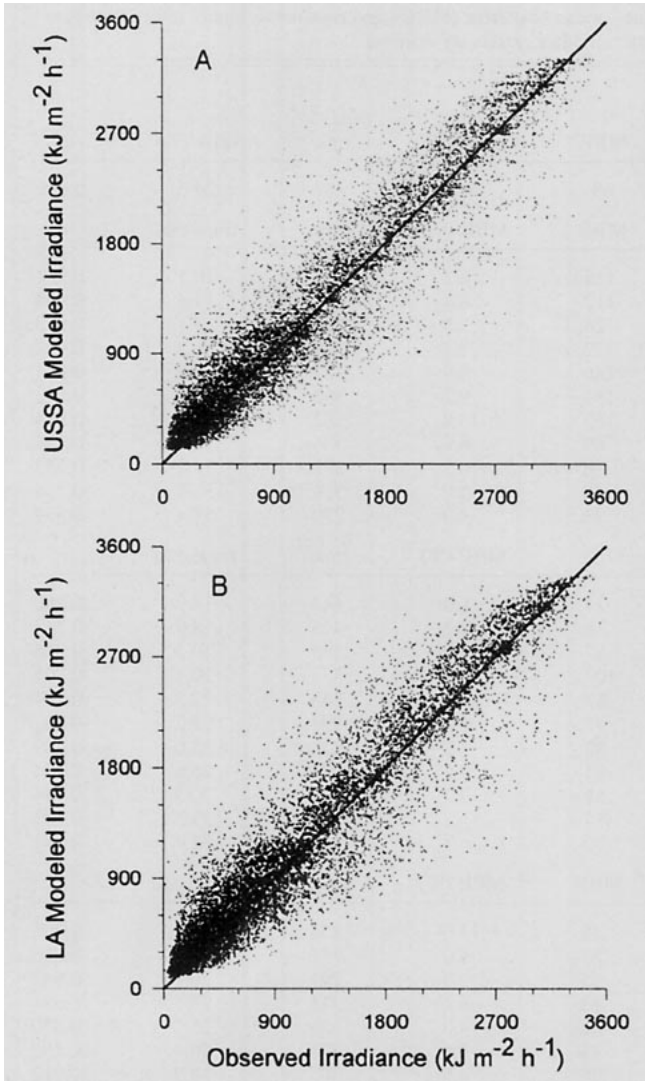

FIG. 2. Comparison of both model runs to observed hourly global irradiance. The line in both panels is the 1:1 line: (a) USSA; (b) LA.

in the SOLMET Volume 2-User's Manual (NCDC 1979).

4. Cloud effects on irradiance

The BR model was modified to include the effects of varying cloud cover on global irradiance. To achieve this extension, mean clear-sky irradiance $\bar{E}(0)$ for each 1° zenith angle bin was calculated from the dataset collected at Sea–Tac. Observed clear-sky irradiance $E(0)$ was defined as that E occurring when total opaque sky cover (TOSC) was equal to 0.0. Zenith angle was calculated according to the formulas given by Iqbal (1983). Irradiance E for each 1° zenith angle bin was then divided by the appropriate $\bar{E}(0)$. This produced a ratio of hourly observed irradiance at any one zenith angle to the hourly clear-sky irradiance at that zenith angle (the global clearness index), which is the proportional reduction in observed irradiance caused by the cloud cover at that hour, assuming all other atmospheric constituents to be equal. Cloud cover effects on clear-sky irradiance as a function TOSC was quantified using the equation of Kasten and Czeplak (1980):

$$\frac{E}{\bar{E}(0)} = 1 - B(\mathrm{TOSC})^A, \qquad (4)$$

where the dimensionless parameter B determines the magnitude of the cloud effect while A, also unitless, controls the shape of the curve (Fig. 1). To determine A and B for the dataset used in this study, the ratio $E/\bar{E}(0)$ was fitted to Eq. (4) using the Levenberg–Marquardt nonlinear algorithm as reported by Press et al. (1992). The value for B was 0.6740 ± 0.0001 (value ± standard error), and A was 2.854 ± 0.002. These values are similar to the values 0.75 and 3.4, respectively, that Kasten and Czeplak (1980) reported for Hamburg, Germany. Figure 1 shows that the algorithm does an adequate job of reproducing the shape of cloud cover effects on clear-sky irradiance.

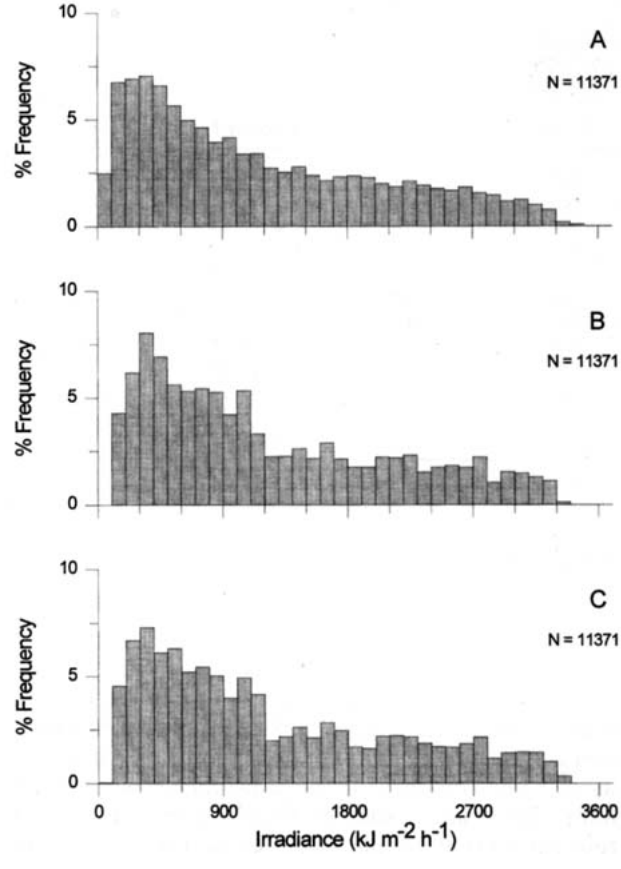

FIG. 3. Frequency distributions of hourly global irradiances as a percentage of the total number of data points: (a) observed; (b) USSA; (c) LA.

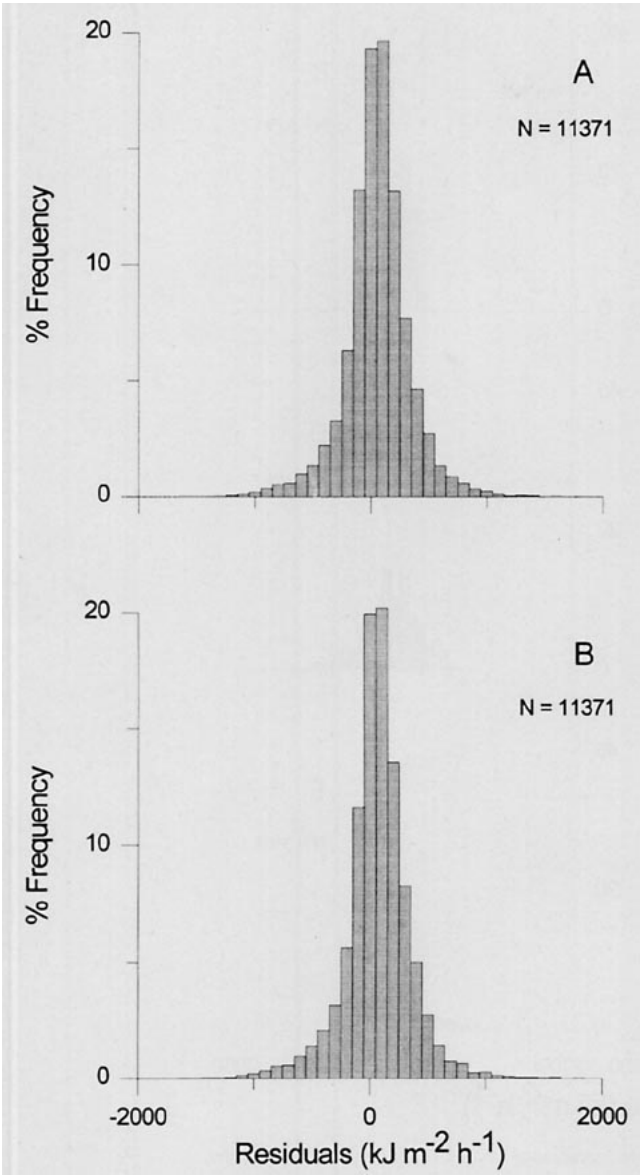

FIG. 4. Frequency distributions of hourly global irradiance residuals (model minus observed) as a percentage of the total number of data points: (a) USSA; (b) LA.

Values of $\hat{E}$ were estimated by modifying the clear-sky irradiances produced by the model $\hat{E}(0)$ according to Eq. (5):

$$\hat{E} = \hat{E}(0)[1 - 0.6740(\mathrm{TOSC})^{2.854}]. \quad (5)$$

5. Comparison of modeled to observed global irradiance

Comparisons between the two modeled datasets and observed global irradiance were performed. In addition, comparisons were made between $\hat{E}_S$ and E and between $\hat{E}_L$ and E as a function of 1) total opaque sky cover to determine the ability of Eq. (4) to adequately remove cloud effects, 2) 5° zenith angle bins for time of day bias, and 3) month of year for seasonal effects. For all comparisons a suite of statistical descriptors were calculated, including the mean and standard deviation of the irradiance values and the mean bias error (MBE), root-mean-square error (rmse), and the squared correlation coefficient (r^2) between the observed and modeled irradiance values. MBE and rmse were both calculated by subtracting the observed irradiance value from the appropriate modeled value; positive values of MBE (the average deviation between two sets of numbers) indicate an overestimation by the model. It is necessary to report both MBE and rmse to determine if the bias in a model is systematic or random. MBE measures systematic error, whereas rmse measures both systematic and random error. A comparison of the two provides insight into a model's performance. These statistical descriptors appear in Tables 3 and 4 for USSA and LA, respectively.

Figure 2 shows the close correspondence between the observed and modeled global irradiance values. Here $\hat{E}$ tended to lie above the 1:1 line, an overestimation tendency confirmed by the positive MBE. The overall MBE for $\hat{E}_S$ was 55.7 kJ m^{-2} h^{-1}, or 4.8% of the observed mean. The MBE for $\hat{E}_L$ was 64.6, or 5.5% of the observed mean. The rmse percentages were virtually identical for both model runs (24.5% and 24.6%). For USSA the r^2 value (the amount of variation explained by a linear model) was 0.899, whereas it was slightly higher for LA at 0.901. In both cases the model was able to explain 90% of the variation in the data. The low MBE and high r^2 values statistically describe what is obvious from Fig. 2, that both model runs do a good job of estimating global irradiance and that the two runs are virtually indistinguishable from each other. The higher rmse than MBE indicates that most of the deviation of modeled from observed values is random in nature.

Figure 3 presents the distribution of irradiance values. The $\hat{E}$ distributions approximate that of E, with the most notable exceptions being at either tail. Neither model run produces the very low or very high values seen in the observed dataset, although the LA run does a slightly better job, as indicated by its slightly higher r^2. Since the USSA is an average atmosphere, it is not surprising that the LA would do better at matching the extremes. Residual distributions are shown in Fig. 4. While both are approximately normally distributed, neither model run has its mode centered on 0 (i.e., in both cases the model overestimates observed irradiance). The shape of the residual distributions explain the slightly higher MBE for LA compared to USSA, with LA being slightly more skewed toward positive residuals.

To determine the primary sources of deviation between E and $\hat{E}$, the dataset was broken into several groupings. Since the MBE, rmse, and r^2 values were approximately the same for both model runs and the

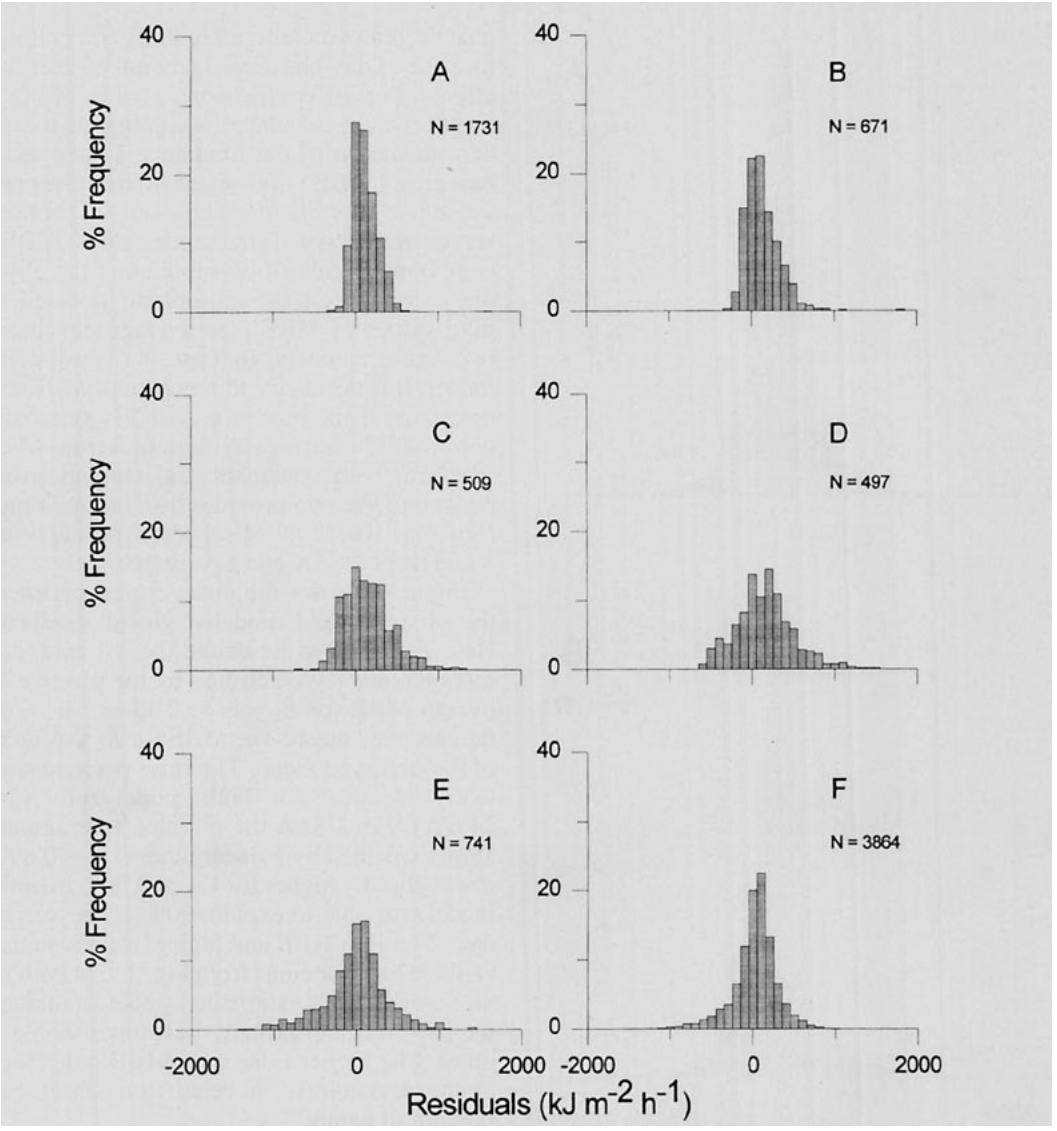

FIG. 5. Frequency distributions of hourly global irradiance residuals for the LA run (model minus observed) as a percentage of the number of data points by TOSC: (a) 0.0; (b) 0.2; (c) 0.4; (d) 0.6; (e) 0.8; (f) 1.0.

distributions of residuals for both were similar in shape, only the results for the LA run are discussed. The first grouping was by TOSC to determine the model's ability to handle cloud effects (Tables 3 and 4, Fig. 5). Of particular interest is the case when TOSC is 0.0. The MBE was approximately the same as for the entire dataset (6.2% vs 5.5%), but the rmse was considerably reduced (10.1% vs 24.6%). This result indicates that the systematic error measured by the MBE of the entire dataset is not primarily due to cloud cover effects but is inherent in the model. Most of the error in the rmse of the entire dataset is nonsystematic in nature and is caused by cloud cover. This result is further supported by the increase observed in rmse (from 10.1% to 54.4%) and the decrease in r^2 (from 0.971 to 0.559) as a function of cloud cover while the MBE showed no trend (Table 4). Figure 5 shows the same result graphically, with the distribution of residuals becoming less skewed to the right as cloud cover increases. Since cloud cover effects on the model are tuned to local opaque conditions for Sea–Tac, the increase in rmse with cloud cover amount is most likely due to variability in types of cloud cover and their respective differing transmissivities, which is not taken into account by the model.

Statistical descriptors and residuals were examined as a function of solar zenith angle in 5° bins for time of day bias. Both MBE and rmse tended to increase with increasing zenith angle, while r^2 showed no consistent pattern (Tables 3 and 4). The increase in MBE

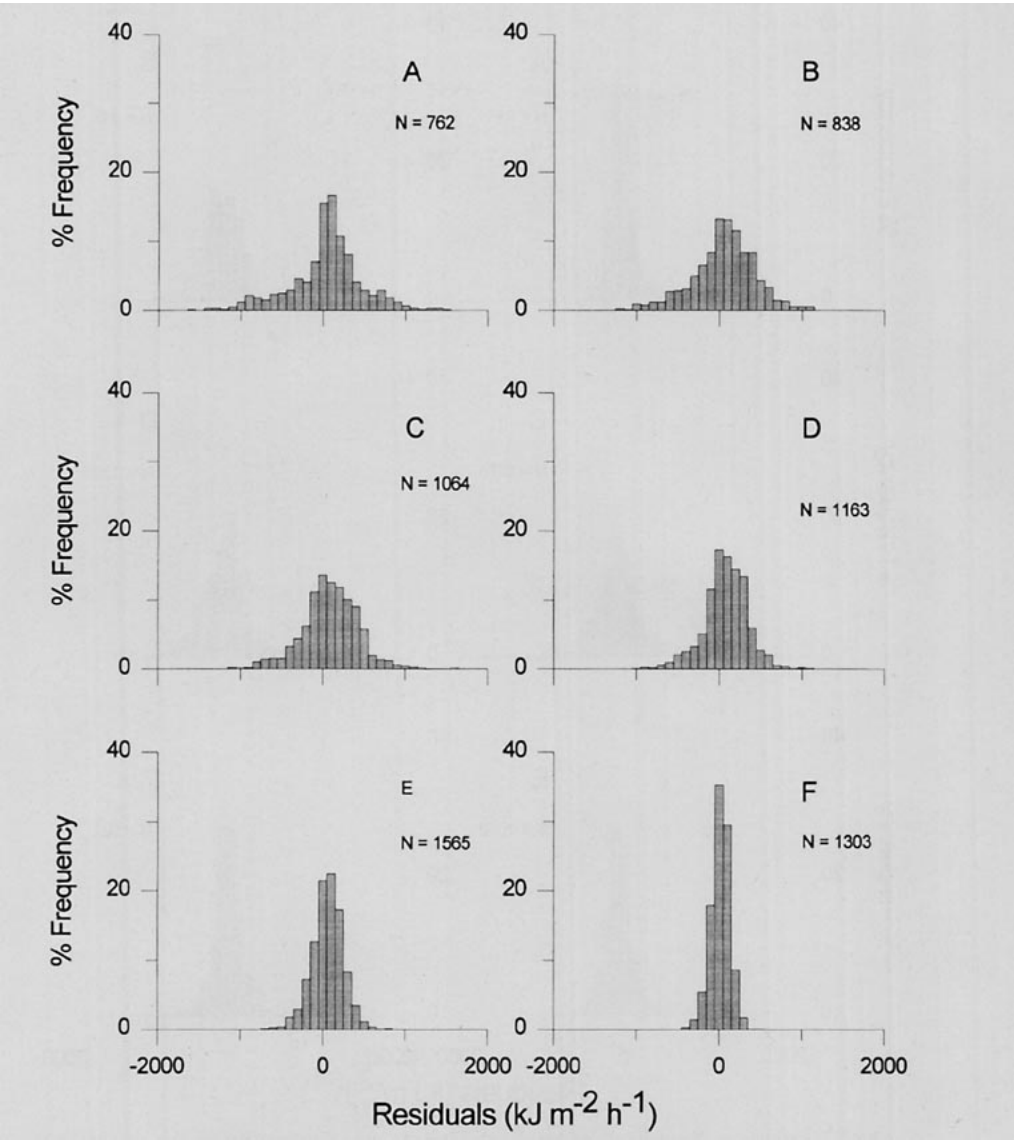

FIG. 6. Frequency distributions of hourly global irradiance residuals for the LA run (model minus observed) as a percentage of the number of data points by 5° zenith angle bins: (a) 25°–30°; (b) 35°–40°; (c) 45°–50°; (d) 55°–60°; (e) 65°–70°; (f) 75°–80°.

and rmse is most likely due to errors in measurement of observed irradiance as the zenith angle increases and global irradiance decreases. The distribution of residuals increased in peakedness with increasing zenith angle (Fig. 6), an effect brought about by the decreasing range of values in both modeled and observed data with higher zenith angles. The model tended to overpredict global irradiance at all zenith angles.

The final data grouping examined was by month in order to determine seasonal effects. All three reported statistical descriptors showed a seasonal effect, with MBE and rmse being high in the winter and low in the summer and r^2 showing the opposite trend (Tables 3 and 4). Summertime in this region sees both a greater range of zenith angles and a decrease in cloud cover, confounding the exact cause of the seasonality in the statistics. An examination of the distribution of residuals in Fig. 7 shows the effects of both causes. The wintertime residuals are markedly peaked as were the residuals for low zenith angles (Fig. 6), whereas the summertime residuals show the positive skewness of lower cloud cover values (Fig. 5). A final cause of seasonality that cannot be ruled out is a change in the cloud cover type over the year that is not explicitly handled in the model.

A careful examination of the trends in the statistical descriptors provides insight into the dominant source of variability between the modeled and observed data

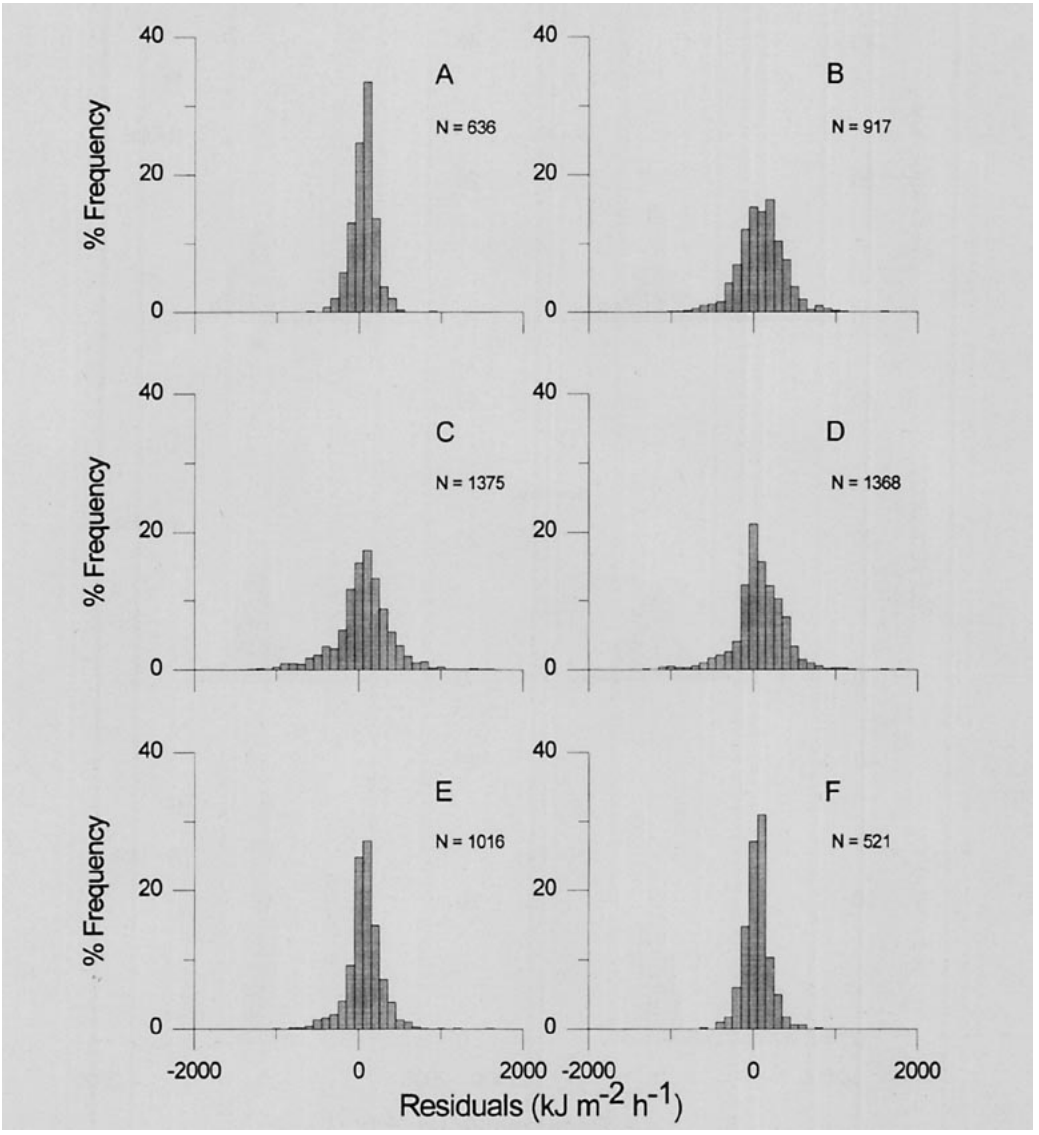

FIG. 7. Frequency distributions of hourly global irradiance residuals for the LA run (model minus observed) as a percentage of the number of data points by month: (a) Jan; (b) Mar; (c) May; (d) Jul; (e) Sep; (f) Nov.

(Tables 3 and 4). In the case of TOSC the trends in mean irradiance and rmse oppose each other while they proceed in the same direction for both zenith angle and month. This scenario is also seen in the r^2 values, whereas MBE shows no definitive trend. This result suggests that the model is inadequate in estimating irradiance under increasingly cloudy skies. Although using total cloud cover to attenuate clear-sky irradiance for oceanographic research has been used in several studies in the past (Reed 1977, 1978, 1982), previous work (Davies and McKay 1982, 1989) has shown that models utilizing cloud-layer information outperform such models. However, cloud-layer information is not always available, particularly in historical datasets such as the Comprehensive Ocean–Atmosphere Data Set (COADS, Woodruff et al. 1987), which can be used to develop a climatology for remote sites.

6. Concluding remarks

For the case of the Seattle–Tacoma airport, there was essentially no difference in the Bird and Riordan (1986) model performance if either the U.S. standard atmosphere values or local meteorological measurements were used as inputs. The BR spectral model estimated hourly clear-sky global irradiance to within an average deviation of 7% of pyranometer measurements taken at the Seattle–Tacoma airport. However, since the weather station reported cloud cover of at least 0.3 more than 70% of the time, the model must be able to

take into account cloud cover in order to be useful. After using local cloud cover data to attenuate estimated clear-sky irradiance, the modified model was still able to hindcast hourly irradiance to within an average deviation of 6% of observed values. It is recommended that, if available, the model should be run with local meteorological observations in order to more closely match the full range of expected values. All of the meteorological inputs to the model, except for cloud cover, are easily measured using relatively inexpensive meteorological instrument packages capable of satellite telemetry. If these observations are unavailable, the model can be run with the USSA, with cloud cover information coming from a climatic data atlas such as COADS. However, it is recommended that the performance of the model using the USSA at the intended geographic location should be verified before use.

Acknowledgments. This manuscript benefited from the comments of J. Campbell, M. Cohen, A. Macklin, J. Napp, R. Reed, and two anonymous reviewers.

REFERENCES

Ångström, A., 1961: Techniques of determining the turbidity of the atmosphere. *Tellus,* **13,** 214–223.

Atwater, M. A., and J. T. Ball, 1976: Comparisons of radiation computations using observed and estimated precipitable water. *J. Appl. Meteor.,* **15,** 1319–1320.

Berthon, J.-F., and A. Morel, 1992: Validation of a spectral light-photosynthesis model and use of the model in conjunction with remotely sensed pigment observations. *Limnol. Oceanogr.,* **37,** 781–796.

Bird, R. E., 1984: A simple spectral model for direct normal and diffuse horizontal irradiance. *Sol. Energy,* **32,** 461–471.

——, and C. Riordan, 1986: Simple solar spectral model for direct and diffuse irradiance on horizontal and tilted planes at the earth's surface for cloudless atmospheres. *J. Climate Appl. Meteor.,* **25,** 87–97.

Davies, J. A., and D. C. McKay, 1982: Estimating solar irradiance and components. *Sol. Energy,* **29,** 55–64.

——, and ——, 1989: Evaluation of selected models for estimating solar radiation on horizontal surfaces. *Sol. Energy,* **43,** 153–168.

Gregg, W. W., and K. L. Carder, 1990: A simple spectral solar irradiance model for cloudless maritime atmospheres. *Limnol. Oceanogr.,* **35,** 1657–1675.

Gueymard, C., 1993: Critical analysis and performance assessment of clear sky solar irradiance models using theoretical and measured data. *Sol. Energy,* **51,** 121–138.

Iqbal, M., 1983: *Introduction to Solar Radiation.* Academic Press, 390 pp.

Justus, C. G., and M. V. Paris, 1985: A model for solar spectral irradiance and radiance at the bottom and top of a cloudless atmosphere. *J. Climate Appl. Meteor.,* **24,** 193–205.

Kasten, F., 1966: A new table and approximate formula for relative optical air mass. *Arch. Meteor. Geophys. Bioklimatol.,* **B14,** 206–223.

——, and G. Czeplak, 1980: Solar and terrestrial radiation dependent on the amount and type of cloud. *Sol. Energy,* **24,** 177–189.

Kneizys, F. X., E. P. Shettle, W. O. Gallery, J. H. Chetwynd Jr, L. W. Abrea, J. E. A. Selby, R. W. Fenn, and R. W. McClatchey, 1980: Atmospheric transmittance/radiance: Computer code LOWTRAN5. Tech. Rep. AFGL-TR-80-0067, USAF Geophysics Laboratory, Hanscom AFB, MA, 233 pp.

Leckner, B., 1978: The spectral distribution of solar radiation at the earth's surface—Elements of a model. *Sol. Energy,* **20,** 143–150.

Louche, A., G. Simonnot, and M. Iqbal, 1988: Experimental verification of some clear-sky insolation models. *Sol. Energy,* **41,** 273–279.

Morel, A., 1991: Light and marine photosynthesis: A spectral model with geochemical and climatological implications. *Progress in Oceanography,* Vol. 26, Pergamon, 263–306.

Nann, S., and C. Riordan, 1991: Solar spectral irradiance under clear and cloudy skies: Measurements and a semiempirical model. *J. Appl. Meteor.,* **30,** 447–462.

National Climatic Center, 1979: SOLMET Vol. 2: Hourly solar radiation—Surface meteorological observations. Final Report, TD-9724, 184 pp.

——, 1991: Surface airways hourly manual. TD-3280, 41 pp.

National Oceanic and Atmospheric Administration, 1976: *U.S. Standard Atmosphere, 1976.* Government Printing Office, 227 pp.

Platt, T., and S. Sathyendranath, 1988: Oceanic primary production: Estimation by remote sensing at local and regional scales. *Science,* **241,** 1613–1620.

Press, W. H., B. P. Flannery, S. A. Teukolsky, and W. T. Vetterling, 1992: *Numerical Recipes: The Art of Scientific Computing.* 2d ed. Cambridge University Press, 963 pp.

Reed, R. K., 1977: On estimating insolation over the ocean. *J. Phys. Oceanogr.,* **7,** 482–485.

——, 1978: Cloud effects on insolation over the tropical Pacific Ocean. *J. Appl. Meteor.,* **17,** 401–404.

——, 1982: Comparison of measured and estimated insolation over the eastern Pacific Ocean. *J. Appl. Meteor.,* **21,** 339–341.

Reitan, C. H., 1960: Distribution of precipitable water over the continental United States. *Bull. Amer. Meteor. Soc.,* **41,** 79–87.

Robinson, N., 1966: *Solar Radiation.* Elsevier, 347 pp.

Selby, J. E., and R. A. McClatchey, 1975: Atmospheric transmittance from 0.25 to 28.5 μm: Computer code LOWTRAN 3. Tech Rep. AFCRL-TR-75-0255, USAF Cambridge Research Laboratories, 109 pp.

Shettle, E. P., and R. W. Fenn, 1975: Models of the atmospheric aerosol and their optical properties. *Proc. Advisory Group for Aerospace Research and Development Conf. 183, Optical Propagation in the Atmosphere,* NATO, 2.1–2.6. Presented at the Electromagnetic Wave Propagation Panel Symp., Lyngby, Denmark.

Smith, W., 1966: Note on the relationship between total precipitable water and surface dew point. *J. Appl. Meteor.,* **5,** 726–727.

van Heuklon, T. K., 1979: Estimating atmospheric ozone for solar radiation models. *Sol. Energy,* **22,** 63–68.

Woodruff, S. D., R. J. Slutz, R. L. Jenne, and P. M. Steurer, 1987: A Comprehensive Ocean–Atmosphere Data Set. *Bull. Amer. Meteor. Soc.,* **68,** 1239–1250.